Amphiphilic 4-Helix Bundles Designed for Biomolecular Materials Applications

Shixin Ye,† Joseph W. Strzalka,† Bohdana M. Discher,‡ Dror Noy,‡ Songyan Zheng,† P. Leslie Dutton,‡ and J. Kent Blasie*,†

Department of Chemistry and Department of Biochemistry & Biophysics, University of Pennsylvania, Philadelphia, Pennsylvania 19104

Received December 17, 2003. In Final Form: April 7, 2004

Artificial peptides previously designed to possess α-helical bundle motifs have been either hydrophilic (i.e., soluble in polar media) or lipophilic (i.e., soluble in nonpolar media) in overall character. Realizations of these bioinspired bundles have succeeded in reproducing a variety of biomimetic functionality within the appropriate media. However, to translate their functionality into any biomolecular device applications at the macroscopic level, the bundles must be oriented in an ensemble, for example, at an interface. This goal has been realized in a new family of α-helical bundle peptides which are amphiphilic; namely, they assemble into 4-helix bundles with well-defined hydrophilic and hydrophobic domains. These peptides are capable of binding metalloporphyrin prosthetic groups at selected locations within these domains. We describe here the realization of one of the first members of this family, AP0, successfully designed for vectorial incorporation into soft interfaces between polar and nonpolar media.

Introduction

Bundles of α-helices provide a scaffold for binding prosthetic groups at selected locations within the structure to mimic functions exhibited by biological proteins.[1−5] For example, histidine residues can be strategically placed for the axial ligation of metalloporphyrin prosthetic groups involved in biological electron-transfer reactions. The first designed artificial peptides used amphipathic dihelices which self-assembled in aqueous solution forming 4-helix bundles. These robust peptides were shown to retain a range of specific functional elements of their natural counterparts by design, but within much more simple structures, and were called "maquettes".[1]

To realize any device applications, the peptides must be vectorially oriented in an ensemble, for example, at an interface. [The three-dimensional structure of the AP0 4-helix bundle is asymmetric. The natural internal coordinate frame is defined by the bundle axis z' with the $x'-y'$ plane containing the helix cross sections. The "vectorial orientation" of the amphiphilic bundle relates this internal coordinate frame (x', y', z') relative to that of the monolayer ensemble (x, y, z). The monolayer coordinate frame can be conveniently defined by the normal z to its plane $x-y$. See ref 6.] Previously, the dihelices of a representative 4-helix bundle, whose sequence was designated "BB", were made amphiphilic via attachment of C16 hydrocarbon chains to their N-termini.[7] BBC16 was shown to undergo a pressure-dependent orientational transition with the helical axes of the bundles changing from parallel to perpendicular to the interface at higher surface pressures.[8−10] This vectorial orientation could be maintained upon the Langmuir−Blodgett deposition of these monolayers onto the nonpolar soft alkylated surface of a solid inorganic substrate.[11] Furthermore, electron transfer was demonstrated between the peptide's prosthetic group(s) and the solid substrate.[12]

However, the amphiphilic BBC16 had certain limitations. The palmitoylated dihelices were unable to form 4-helix bundles at the air−water interface.[13] The Langmuir monolayers of pure BBC16 were also somewhat unstable at higher surface pressures. The instability of the pure BBC16 monolayers was substantially improved by utilizing mixed monolayers of the peptide with the phospholipid (dilauroylphosphatidylethanolamine, DLPE).[9] A more serious limitation for the BBC16 type of amphiphilic maquette was its inability to generate vectorial function, for example, electron transfer between metalloporphyrin prosthetic groups and thereby electric charge separation, across an interface between polar and nonpolar media.

To generate vectorial function across an interface, two approaches have been investigated, designed to render the 4-helix bundle maquettes themselves amphiphilic, namely, to possess both a hydrophilic and a hydrophobic domain. In the first case, each α-helix is again designed to be amphipathic with polar and nonpolar faces, but the sequence was such that if the nonpolar faces of each amphipathic helix were apposed in the 4-helix bundle over the first m-residues of each helix, the polar faces would

† Department of Chemistry.

‡ Department of Biochemistry & Biophysics.

(1) Robertson, D. E.; Farid, R. S.; Moser, C. C.; Urbauer, J. L.; Mulholland, S. E.; Pidikiti, R.; Lear, J. D.; Wand, A. J.; Degrado, W. F.; Dutton, P. L. *Nature* **1994**, *368*, 425−431.

(2) Rabanal, F.; DeGrado, W. F.; Dutton, P. L. *J. Am. Chem. Soc.* **1996**, *118*, 473−474.

(3) Sharp, R. E.; Moser, C. C.; Rabanal, F.; Dutton, P. L. *Proc. Natl. Acad. Sci. U.S.A.* **1998**, *95*, 10465−10470.

(4) Gibney, B. R.; Rabanal, F.; Skalicky, J. J.; Wand, A. J.; Dutton, P. L. *J. Am. Chem. Soc.* **1999**, *121*, 4952−4960.

(5) Gibney, B. R.; Huang, S. S.; Skalicky, J. J.; Fuentes, E. J.; Wand, A. J.; Dutton, P. L. *Biochemistry* **2001**, *40*, 10550−10561.

(6) Chupa, J. A.; McCauley, J. P.; Strongin, R. M.; Smith, A. B., III; Blaise, J. K.; Peticolas, L. J.; Bean, J. C. *Biophys. J.* **1994**, *67*, 336−348.

(7) Chen, X. X.; Moser, C. C.; Pilloud, D. L.; Dutton, P. L. *J. Phys. Chem. B* **1998**, *102*, 6425−6432.

(8) Tronin, A.; Strzalka, J.; Chen, X.; Dutton, P. L.; Ocko, B. M.; Blaise, J. K. *Langmuir* **2001**, *17*, 3061−3066.

(9) Strzalka, J.; Chen, X. X.; Moser, C. C.; Dutton, P. L.; Ocko, B. M.; Blasie, J. K. *Langmuir* **2000**, *16*, 10404−10418.

(10) Blasie, J. K.; Timmins, P. *MRS Bull.* **1999**, *24*, 40−47.

(11) Strzalka, J.; Chen, X. X.; Moser, C. C.; Dutton, P. L.; Bean, J. C.; Blasie, J. K. *Langmuir* **2001**, *17*, 1193−1199.

(12) Pilloud, D. L.; Rabanal, F.; Gibney, B. R.; Farid, R. S.; Dutton, P. L.; Moser, C. C. *J. Phys. Chem. B* **1998**, *102*, 1926−1937.

(13) Ye, S.; Strzalka, J.; Chen, X.; Moser, C. C.; Dutton, P. L.; Ocko, B. M.; Blasie, J. K. *Langmuir* **2003**, *19*, 1515−1521.

10.1021/la0363884 CCC: $27.50
Published on Web 06/05/2004

Chart 1. Schematic Illustration of AP0[a]

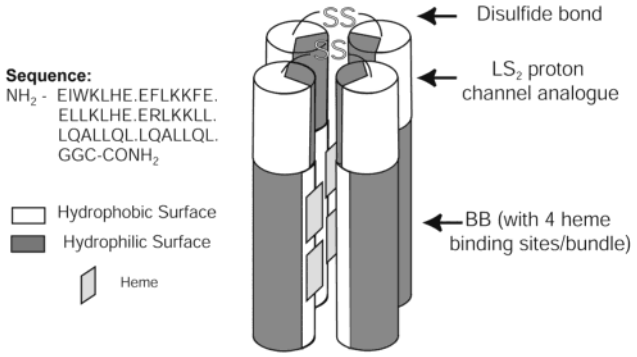

[a] The relatively hydrophilic BB sequence is elongated with two heptads of a more hydrophobic sequence taken from the artificial proton channel protein LS_2. The helices remain amphipathic over their entire length, although the polar and nonpolar faces are reversed between the four heptads of the BB sequence relative to the two heptads of the LS_2 sequence. The C-terminal cysteine is oxidized to form a disulfide bond between two helices to make dihelices.

be apposed over the last *n*-residues. Thus, a 4-helix bundle of parallel (or syn) topology would possess a charged-polar exterior with a nonpolar interior over the first *m*-residues thereby forming the hydrophilic domain and a nonpolar exterior with an uncharged-polar interior over the last *n*-residues thereby forming the hydrophobic domain of the maquette. The first of these amphiphilic 4-helix bundles was designated AP0 (for amphiphilic protein zero). The hydrophilic portion of the bundle was modeled after the representative hydrophilic maquette using four heptads of the sequence "BB", and the hydrophobic portion of the bundle was modeled using two heptads of a synthetic proton channel[14] to result in AP0, as shown in Chart 1. AP0 can possess bis-histidyl metalloporphyrin binding sites at two positions of the sequence separated by 14 residues within the larger hydrophilic portion of the 4-helix bundle.

In this communication, we focus on an important realization of these design principles, namely, the design, assembly, functional characterization, and surface properties of AP0 as a prototypical member of this new family of amphiphilic maquettes. In separate communications, we describe the design and characterization of the other three of this family of amphiphilic 4-helix bundle peptides, AP1, AP2, and AP3. These amphiphilic peptides represent the second case in which the hydrophobic portion of the bundle was modeled utilizing either four heptads of the relatively hydrophobic helix of the influenza M2 transmembrane domain[15] or two heptads of cytochrome *b*'s hydrophobic transmembrane helix within the cytochrome bc_1 complex.[16] Like AP0, AP1 can possess bis-histidyl metalloporphyrin binding sites within the hydrophilic portion of the 4-helix bundle. Importantly, both AP2 and AP3 also possess bis-histidyl metalloporphyrin binding sites in the hydrophobic portion of the bundle.

The "modular design" principles employed here for the amphiphilic 4-helix bundles designated AP0−AP3 have been described in a recent publication.[17] In addition, we further demonstrate that in binary mixtures with phospholipids, these amphiphilic bundles vectorially orient in Langmuir monolayers at lower surface pressures due to the insertion of the nonpolar exterior of the bundle into the host phospholipid monolayer.[18] These two new types of amphiphilic 4-helix bundles now allow for the positioning of prosthetic groups on either side of the interface. This is essential for the vectorial electron transfer across the interface to create an electrochemical potential, thereby transforming a designed molecular property at the microscopic level into a material property of the interface at the macroscopic level.

Materials and Methods

Synthesis. The peptide (NH_2−^{1}EIWKLHE.EF^{10}LKKFE.ELLKL^{20}HE.ERLKKLL.L^{30}QALLQL.LQAL^{40}LQL.GGC−$CONH_2$)-was synthesized on Applied Biosystems' Pioneer continuous flow solid phase synthesizer using standard Fmoc/tBu protection strategy on a Fmoc−PEG−PAL−PS resin (Applied Biosystems) at 0.1 mmol scale. The peptides were acetylated at their N-terminus (1:1 (v/v) acetic anhydride−pyridine for 30 min) and purified on a reversed phase C_4 HPLC column (Vydac) using gradients of 6:3:1 2-propanol/acetonitrile/H_2O (solvents from Fisher) and water containing 0.1% (v/v) TFA (Sigma). Pure peptides (5.40 kDa molecular weight) were dimerized by oxidizing the C-terminal cysteines in 1:1 (v/v) 100 mM ammonium hydrogen carbonate buffer (pH 10.0) and methanol in air to form the 90 amino acid disulfide-linked peptide dimer (10.79 kDa molecular weight). The peptide's identity and purity were confirmed by matrix-assisted laser desorption/ionization time-of-flight mass spectrometry (MALDI-TOF).

Protein Characterizations. *UV−Vis Absorbance and Circular Dichroism Spectroscopy.* Peptide samples were measured in buffered aqueous solutions containing 0.9% *n*-octyl β-D-glucopyranoside (OG) (Sigma), 10 mM sodium phosphate, and 100 mM potassium chloride at pH 8.0. Peptide concentrations were determined by absorption at 280 nm assuming an extinction coefficient of 5690 M^{-1} cm^{-1} calculated from sequence by the EXPASY server of the Swiss Institute of Bioinformatics (http://us.expasy.org/cgi-bin/protparam). A Perkin-Elmer Lambda 2 spectrophotometer and a standard 1 cm path length quartz cuvette were used for absorbance measurements. Circular dichroism (CD) spectra were recorded with an Aviv 62DS spectropolarimeter in rectangular quartz cells of 2 mm path length for peptide concentrations between 10 and 15 μM.

Heme Incorporation and Redox Potentiometry. A dimethyl sulfoxide (DMSO) (Aldrich) solution of heme (Sigma) was added in 0.1 equiv aliquots to peptides in 0.9% OG solutions. The final concentration of DMSO in the peptide solution was lower than 2% (v/v). The values of the dissociation constants, K_d, were determined by monitoring changes in the heme visible absorbance as previously described.[19] The reduction potential of the first heme bound to an AP0 bundle was also determined as described previously.[19] The data were fit to a single Nernst equation with $n = 1.0$ (fixed).

Analytical Ultracentrifugation. Sedimentation equilibrium experiments were performed at 25 °C on peptides solubilized in 0.9% OG pH 8.0 buffered solution using a Beckman XLA/I analytical ultracentrifuge. The method of Noy et al.[20] was used in order to resolve the contribution of detergent and peptide molecules to the molecular weight of the peptide−detergent complex. Apo-AP0 as a four-helix bundle would have a molecular weight of 21.59 kDa and a theoretical partial specific volume of 0.789 mL/g (calculated from its sequence using the amino acid residue parameters of Kharakoz[21] substituted for the Cohn & Edsall parameters[22] in the program Sednterp).[23] The molecular

(14) Lear, J. D.; Wasserman, Z. R.; Degrado, W. F. *Science* **1988**, *240*, 1177−1181.
(15) Huang, S. S.; Koder, R. L.; Lewis, M.; Wand, A. J.; Dutton, P. L. *Proc. Natl. Acad. Sci. U.S.A.*, in press.
(16) Iwata, S.; Lee, J. W.; Okada, K.; Lee, J. K.; Iwata, M.; Rasmussen, B.; Link, T. A.; Ramaswamy, S.; Jap, B. K. *Science* **1998**, *281*, 64−71.
(17) Discher, B.; Koder, R.; Moser, C. C.; Dutton, P. L. *Curr. Opin. Struct. Biol.* **2003**, *7*, 741−748.
(18) Ye, S.; Discher, B.; Strzalka, J.; Noy, D.; Zheng, S.; Dutton, P. L.; Blaise, J. K. Manuscript in preparation.
(19) Chen, X. X.; Discher, B. M.; Pilloud, D. L.; Gibney, B. R.; Moser, C. C.; Dutton, P. L. *J. Phys. Chem. B* **2002**, *106*, 617−624.
(20) Noy, D.; Calhoun, J. R.; Lear, J. D. *Anal. Biochem.* **2003**, *320*, 185−192.
(21) Kharakoz, D. P. *Biochemistry* **1997**, *36*, 10276−10285.
(22) Cohn, E. J.; Edsall, J. T. *Proteins, Amino Acids, and Peptides*; Reinhold: New York, 1943.

weight of a four-helix bundle holo-AP0 incorporating one heme molecule would similarly be 22.21 kDa, and assuming a partial specific volume for heme[24] of 0.82 mL/g, its theoretical partial specific volume would be 0.791 mL/g.

Samples were measured simultaneously in a series of buffered D_2O/H_2O solutions (v/v, 20%, 40%, 60%, 80%, 90%, and 100%) corresponding to solvent densities of 1.0205, 1.0420, 1.0635, 1.0849, 1.0957, and 1.1064 g/mL, respectively (calculated from buffer composition using the program Sednterp). The total protein concentration was 0.275 mg/mL (52 μM/α-helix).

Radial profiles of absorbance at 280 nm for apo-AP0 and 412 nm for hemo-AP0 were collected at 40 000 rpm at 25 °C for each sample. Data were collected 14 and 16 h after setting the desired speed, and equilibrium conditions were assumed after verifying that the early and late data sets are the same. The data were analyzed by a nonlinear global fit procedure, in which six experimental data sets were fit simultaneously as previously described.[20] A custom program package written with Igor Pro software (version 4.07, Wavemetrics, Inc., Lake Oswego, OR), incorporating Igor Pro's curve-fit functions and global-fitting package, was used for data analysis.

Langmuir Trough and Isotherm Measurements. We spread protein monolayers on a Langmuir trough (R&K, Germany), fabricated from a copper block and coated with Teflon, with the aqueous subphase which contained 1 mM potassium phosphate and 10 mM KCl at pH 8.0. The temperature of the subphase was controlled at 20 °C and maintained by cooled water circulation in the copper block during the experiment. Surface pressure was measured by a Wilhelmy plate and controlled by a movable barrier with feedback. Since high-quality X-ray reflectivity data can only be obtained from Langmuir monolayers when the aqueous subphase surface is relatively smooth, the Langmuir trough sat on a vibration isolation stage in the liquid-surface spectrometer described below, a delay time of several seconds was employed between any motion of the spectrometer and data collection, and a flat smooth glass block was also submerged slightly below the water surface to damp long-wavelength excitations in the local height of the water surface. During the X-ray reflectivity measurements, moist helium gas was circulated inside the trough to replace the air, thereby reducing the X-ray background scattering and minimizing subphase evaporation.

Proteins were dissolved in methanol and spread directly, and the total volume of the deposition solution was in the range of 300−400 μL. Compression at a constant rate of 15 mm/min proceeded after a 10 min wait to allow for the evaporation of organic solvent, until the desired surface pressure was achieved and then maintained constant during the X-ray measurements.

Liquid-Surface Spectrometer. The X-ray reflectivity experiments were performed on beamline X-22B at the National Synchrotron Light Source (NSLS) at Brookhaven National Laboratory, Upton, NY. Details of the liquid-surface spectrometer have been reported elsewhere.[25,26] Here we give only a brief description. The synchrotron X-ray source was a bending-magnet in the electron storage ring operating at an energy of 2.8 GeV and currents of 150−250 mA. Monochromatic X-rays were obtained via a horizontally reflecting Si(111) crystal monochromator to provide a wavelength $\lambda = 1.546$ Å. X-rays were reflected downward onto the horizontal liquid surface via a Ge(111) crystal to provide an angle of incidence α. Incident beam slits were set to collect the full horizontal width and vertically to limit the footprint on the liquid surface. A scintillation detector recorded the scattering from a thin Kapton film in the incident beam to provide an incident beam flux monitor. The specularly reflected beam from the liquid surface was measured at an angle β with respect to the liquid surface with another scintillation detector for $\alpha = \beta$ in the vertical scattering plane at $2\theta_{xy} = 0°$. Scattered beam slits were set to accept the full specularly reflected beam. Off-specular background was measured at $\alpha = \beta$ with $2\theta_{xy} = \pm 10.3°$. The difference (specular minus off-specular background) provided the reflectivity $R(q_z)$ for photon momentum transfer q_z perpendicular to the liquid surface with $q_z = (4\pi/\lambda) \sin \alpha$.

Data Analysis. The Fresnel normalized specular X-ray reflectivity $R(q_z)/R_F(q_z)$ from a liquid surface arises from, in the first Born approximation, the modulus square of the Fourier transform of the gradient (or derivative) $d\rho(z)/dz$ of the electron density profile $\rho(z)$ across the air−water interface averaged over the in-plane coherence length of the incident X-rays,[27,28] namely,

$$R(q_z)/R_F(q_z) = |(\rho_\infty^{-1}) \int [d\rho(z)/dz] \exp(i\, q_z' z)\, dz|^2 \equiv |F(q_z')|^2 \quad (1)$$

where the $R_F(q_z)$ is Fresnel reflectivity from a single infinitely sharp (ideal) interface, the electron density of the semi-infinite bulk subphase is ρ_∞, and q_c is q_z at the critical angle for the subphase α_c. This expression, eq 1, becomes progressively less valid as q_z approaches q_c, which is mitigated to some extent in the distorted wave Born approximation by the use of q_z', where $(q_z')^2 = [(q_z)^2 - (q_c)^2]$.[29] The normalized reflectivity data were analyzed by the box-refinement method, which requires no a priori assumptions and is therefore model-independent. This approach has been utilized previously by us[9,30,31] and is presented in rigorous detail in a recent publication.[32]

Results

Design of the Amphiphilic Peptide AP0. AP0 is a chimera of the designed, water-soluble BB maquette peptide and an analogue of synthetic transmembrane proton channel LS_2.[14] Chart 1 shows the architecture of the AP0. Residues 1−27 of AP0 are derived from the designed peptide BB, which is the homodimer (via a Cys−Cys disulfide bond) of the following sequence:[4]

^{1}CGGG.EIWKL^{10}HE.EFLKKFE.E^{20}LLKLHE.
ERLK^{30}KL

The histidine residues providing axial ligands for two heme binding sites originally denoted as the H10 and H24 positions in the BB sequence are preserved in AP0 to incorporate hemes, and they correspond to positions 6 and 20 in AP0, respectively, due to the deletion of 4 residues at the N terminus.

The two C-terminal heptads (residues 29−42) are based on the design of the synthetic proton channel, LS_2 (H_2N−(Leu-Ser-Leu-Leu-Leu-Ser-Leu)$_3$−$CONH_2$). We replace the serine in the LS_2 with glutamine to incorporate hydrogen bonding in the interior of the hydrophobic domain and thereby induce proper assembly of the protein. It is believed that hydrogen bonds within the core region of the helices provide remarkably strong association force.[33,34] A leucine (residue 28) was inserted between the BB and LS_2 sequences to match hydrophobicity/hydrophilicity alignment in the core region of the 4-helix bundle. At the end of the hydrophobic region, we added 2 Gly and

(23) Laue, T.; Shaw, B. D.; Ridgeway, T. M.; Pelletier, S. L. *Computer-aided interpretation of analytical sedimentation data for proteins*; The Royal Society of Chemistry: Cambridge, U.K., 1992.

(24) Mayer, G.; Anderka, O.; Ludwig, B.; Schubert, D. *Progress in Colloid and Polymer Science*; Springer-Verlag Heidelberg: Heidelberg, Germany, 2002; Vol. 119, pp 77−83.

(25) Weiss, A. H.; Deutsch, M.; Braslau, A.; Ocko, B. M.; Pershan, P. S. *Rev. Sci. Instrum.* **1986**, *57*, 2554−2559.

(26) Braslau, A.; Pershan, P. S.; Swislow, G.; Ocko, B. M.; Als-Nielsen, J. *Phys. Rev. A* **1988**, *38*, 2457−2470.

(27) Helm, C. A.; Tippmann-krayer, P.; Möhwald, H.; Als-Nielsen, J.; Kjaer, K. *Biophys. J.* **1991**, *60*, 1457−1476.

(28) Als-Nielsen, J.; Pershan, P. S. *Nucl. Instrum. Methods Phys. Res.* **1983**, *208*, 545−548.

(29) Lösche, M.; Piepenstock, M.; Diederich, A.; Grunewald, T.; Kjaer, K.; Vaknin, D. *Biophys. J.* **1993**, *65*, 2160−2177.

(30) Zheng, S.; Strzalka, J.; Jones, D. H.; Opella, S. J.; Blasie, J. K. *Biophys. J.* **2003**, *84*, 2393−2415.

(31) Zheng, S. Y.; Strzalka, J.; Ma, C.; Opella, S. J.; Ocko, B. M.; Blasie, J. K. *Biophys. J.* **2001**, *80*, 1837−1850.

(32) Blasie, J. K.; Zheng, S.; Strzalka, J. *Phys. Rev. B* **2003**, *67*, 224201-8.

(33) Choma, C.; Gratkowski, H.; Lear, J. D.; DeGrado, W. F. *Nat. Struct. Biol.* **2000**, *7*, 161−166.

(34) Zhou, F. X.; Cocco, M. J.; Russ, W. P.; Brunger, A. T.; Engelman, D. M. *Nat. Struct. Biol.* **2000**, *7*, 154−160.

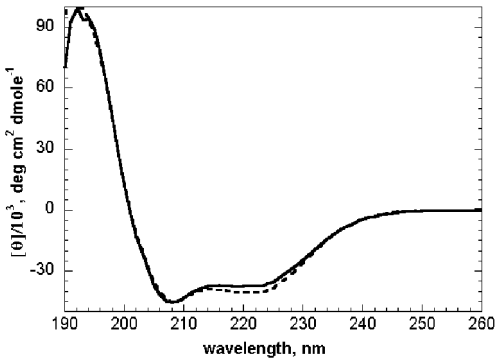

Figure 1. CD spectra of AP0 in methanol (solid) and 4.5% OG, 50 mM KPi (pH 8.0) (dashed). The characteristic maximum at 192 nm and minima at 208 and 222 nm indicate that AP0 is α-helical in the presence of methanol and detergent micelles. The observed spectral features suggest 70−80% helix formation.

a terminal Cys to follow the original BB design to form dihelices via a covalent disulfide linkage.

Peptide Secondary Structure. AP0 peptide is soluble in methanol and aqueous buffer in the presence of detergent. The structural studies employing Langmuir monolayers were done by spreading peptide from methanol solution. Other structural and functional characterizations were conducted in detergent−buffer solution. Therefore, we studied the secondary structure of AP0 in both methanol and detergent micelles using CD spectroscopy. Figure 1 displays the far-UV circular dichroism spectra of AP0 in methanol and phosphate buffer with 0.9% OG, which are typical of highly α-helical peptides (70−80% helical content) with characteristic minima at 208 and 222 nm (arising from the $\pi \rightarrow \pi^*$ and $n \rightarrow \pi^*$ transition of α-helical systems, respectively) and a maximum at 192 nm.

Peptide Aggregation States. The association states of both the apo- and holo- forms of AP0 in detergent micelles were examined using analytical ultracentrifugation. To avoid the presence of free heme in the system, a stoichiometry of one heme/4-helix bundle is chosen to study the aggregation state of the holo- form. Only the first and tightest binding site should be occupied. Fixing the partial specific volume at 0.789 mL/g, as calculated from the peptide sequence, yields a molecular weight of 15.9 ± 0.9 kDa, which is not an integer multiple of the monomeric dihelices species, and a reasonable detergent/sedimenting-species mole ratio[20] of 34.3 ± 12.8. These results suggest that apo-AP0 consists of an equilibrium mixture of the monomeric dihelices species and higher oligomers, the latter dominated by 4-helix bundles since the average molecular weight is intermediate between that of monomers and dimers of the dihelices. On the other hand, the sedimentation equilibrium data of holo-AP0 (Figure 2b), fixing the partial specific volume at 0.789 mL/g, yields a molecular weight of 21.2 ± 0.2 kDa, which agrees with the molecular weight of the 4-helix bundle, and a reasonable detergent/sedimenting-species ratio[20] of 72.3 ± 2.1. Similar results were obtained when the disulfide linkage forming the dihelices was not present; namely, the apo-form of AP0 appears to consist of an equilibrium mixture of 2-helix and 4-helix bundles while the holo- form consists of only 4-helix bundles.

Heme−Peptide Dissociation Constants and Redox Potential. To assess the specificity of heme binding to the peptide, we used UV−vis absorption spectroscopy. The AP0 sequence contains two histidine residues which can serve as axial ligands to the heme iron atom. To avoid complexity due to binding of 4 hemes per 4-helix bundle of AP0, we synthesized an AP0 variant, denoted as AP0-H6A20, in which the His20 is substituted by an Ala. Hemin B (250 μM) [ferric (protoporphyrin IX)Cl] in DMSO was

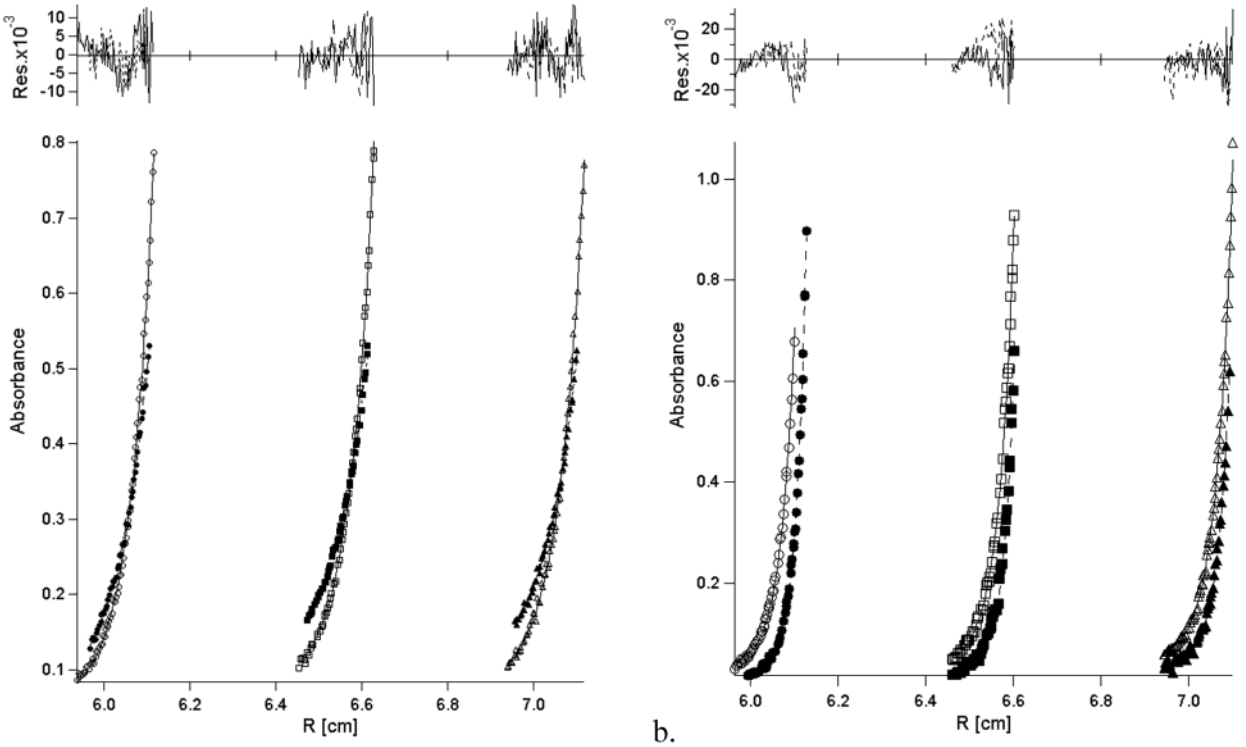

Figure 2. Simultaneous nonlinear fits of sedimentation equilibrium radial absorbance profiles of AP0 in the absence (a) and presence (b) of one heme/4-helix bundle in 0.9% OG, 10 mM KPi, 100 mM KCl pH = 8.0 buffer for raw data (symbols) and their global fits (solid and dotted lines) at D_2O/H_2O 20% (●), 40% (■), 60% (▲), 80% (○), 90% (□), and 100% (△) at 40 000 rpm. The residuals for each fit appear above the radial absorbance profiles. The fitting of hemo-AP0 agrees with a single 4-helix bundle species with a reasonable detergent/peptide ratio of 102.2 ×b1 3.3.

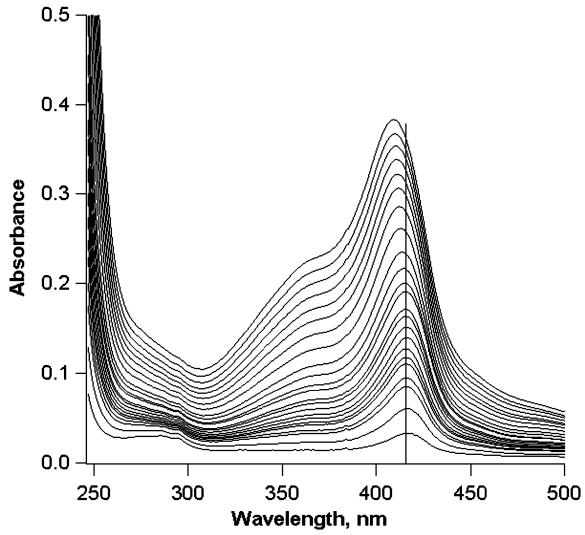

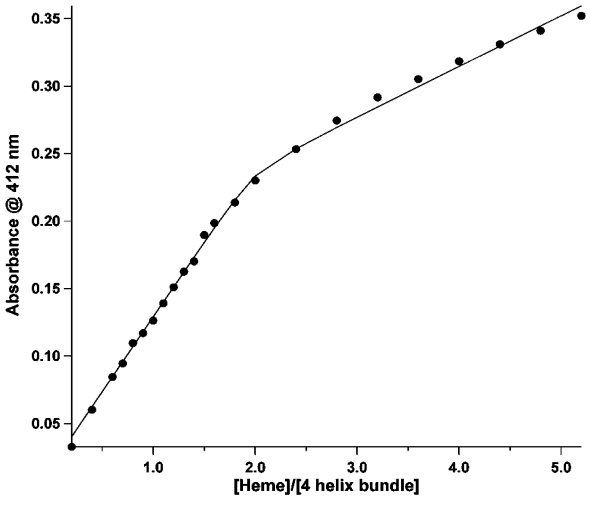

Figure 3. Titration of hemin into a 1.0 μM solution of AP0 recorded in a 1 cm path length cuvette. (a) The spectra shown contain 0.20, 0.40, 0.60, 0.70, 0.80, 0.90, 1.00, 1.10, 1.20, 1.30, 1.40, 1.50, 1.60, 1.80, 2.00, 2.40, 2.80, 3.20, 3.60, 4.00, 4.40, 4.80, and 5.20 equiv of added hemin per 4-helix bundle. A vertical line at peak 412 nm indicates the blue-shift of the peak, which is due to the contribution of free heme (absorption at 400 nm) in the solution. (b) Heme binding determined from the absorbance at 412 nm vs [heme/4-helix bundle] ratio. Fitting two dissociation constants yielded tight $K_{d1} \leq 1$ nM (which is not more accurately determined at this peptide concentration) and $K_{d2} = 30$ nM.

titrated into AP0-H6A20 solutions with a 4-helix bundle concentration of 1.0 μM. Gentle agitation results in incorporation of heme into the bundle, as evidenced by an increase in the Soret maximum at 412 nm (ϵ of 1.20×10^5 M^{-1} cm^{-1} $heme^{-1}$) (Figure 3a) and poorly resolved α and β bands at 535 nm (not shown). Fitting the data to a two-binding-constant equilibrium equation gives a tighter K_{d1} on the sub-nM range and K_{d2} of 30 nM (Figure 3b). BB and its variants all have a tighter K_{d1} ranging from <0.5 to 50 nM and K_{d2} from 35 to 800 nM.[35,36] These values indicate the binding environments of AP0 for the first two hemes are similar to BB and its variants.

The room-temperature midpoint potential of the tightest bound heme (one heme/4-helix bundle with sub-nM K_d) in AP0 was determined to be -146 ± 2 mV versus standard hydrogen electrode (SHE) (Figure 4) in 10 mM sodium phosphate and 100 mM KCl at pH 8.0. The value is about 40 mV higher than the midpoint potential for the first

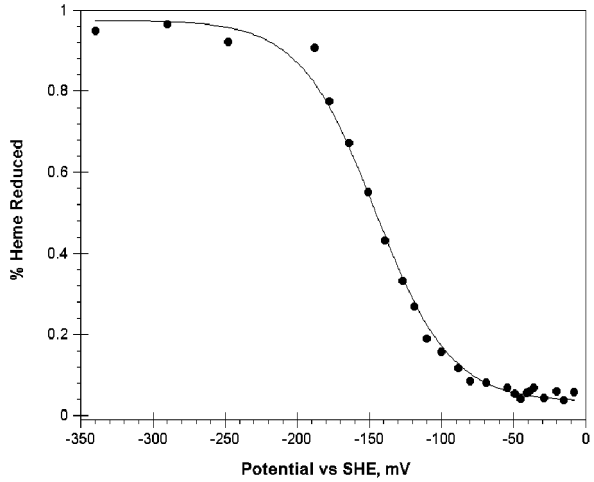

Figure 4. The redox titration curve of the one heme bound per 4-helix bundle of AP0 monitored by optical spectroscopy at 25 °C. The fraction of heme reduced was determined by the change in absorbance at 560 nm relative to an isosbestic point (576 nm) with this difference normalized to 1 for the fully reduced case. The solid line represents a Nernst equation fit to the experimental data points, and it gives the midpoint potential of -146 ± 2 mV. Reduction potentials are reported relative to SHE.

heme bound to BB (−190 mV),[36] which suggests that the local environment for the heme in AP0 is somewhat more hydrophobic than BB.

Langmuir Surface Pressure−Area Isotherms. Figure 5a compares isotherms for apo- and hemo- forms of AP0, with the soluble di-α-helical peptide BB and its derivative BBC16, which was made amphiphilic through the addition of C16 hydrocarbon chains to the N-terminus of each helix.[7,9] Although the water-soluble bundle BB can be spread at the air/water interface and even compressed to high surface pressure (π), the area/α-helix at high π is unreasonably small, less than 100 Å^2, the smallest cross-sectional area of an ideal single helix. More importantly, it was not possible to maintain the monolayer at high π for reflectivity measurements,[9] since molecules enter the subphase rather than remain at the interface. The hydrophobic C16 chains of BBC16 anchored the peptide at the interface, and the monolayer could be maintained at high π with an area/α-helix consistent with the cross-sectional area of helices oriented approximately normal to the interface, as X-ray reflectivity confirmed.[9] AP0 can be compressed to $\pi > 40$ mN/m and maintained at that pressure with a minimum area of about 200 Å^2 per helix. This is only slightly larger than the minimum cross-sectional area of a single helix derived from the NMR structure of BB, which indicates a helical diameter[37] of 12−13 Å^2 and corresponding cross-sectional area of 144−170 Å^2. The isotherm of apo-AP0 has two inflection points (where the curvature changes sign) like the isotherms for apo-BBC16, but the intervening region in between (300 Å^2 < area < 700 Å^2) is not as close to horizontal as the plateau region in apo-BBC16, which arises from an orientational phase transition between helices oriented parallel to the air/water interface and helices oriented normal to the interface, as demonstrated by X-ray reflectivity.[9] The isotherm of apo-AP0 also contains two inflection points, implying a similar transition (supported by X-ray data presented below), though less abrupt. This is probably because unlike BBC16, the amphipathicity of AP0 is not constant over the length of its helices but reverses polarity, which would tend to destabilize the

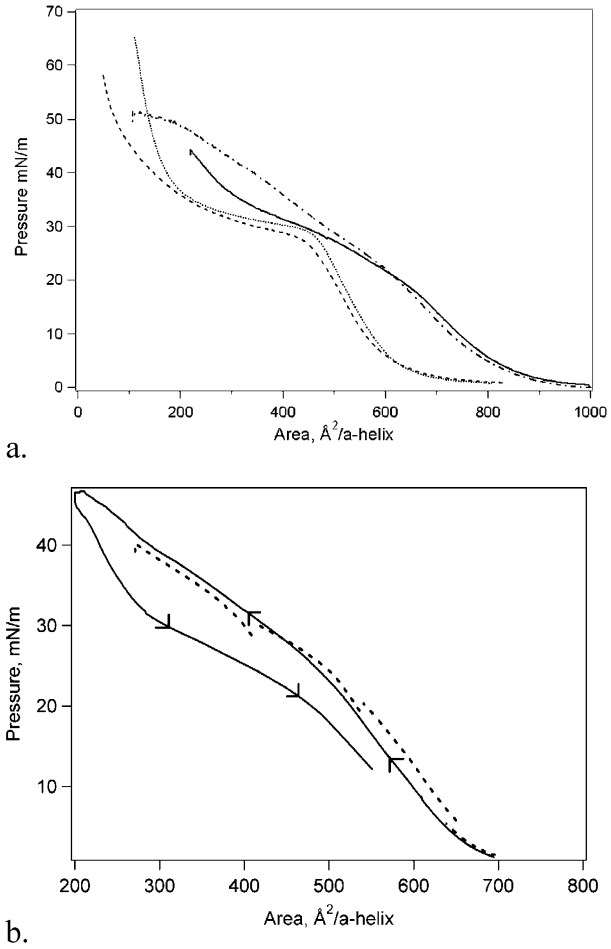

Figure 5. (a) Surface pressure−area isotherms of pure peptide monolayers: apo-AP0 (solid), holo-AP0 (dash−dot), apo-BBC16 (dot), and apo-BB (dash). AP0 was spread on a 1 mM phosphate/10 mM KCl buffer subphase, pH 8.0 at 20 °C; BB and BBC16 were spread on 1 mM phosphate buffer, pH 8.0 at 10 °C. (b) Continuous compression and expansion cycle of apo-AP0 on the same subphase (solid) and data collected in intervals with pauses to collect reflectivity data, showing good stability of the monolayer.

orientation of the helices parallel to the interface, as each helix cannot have its polar and nonpolar surfaces in contact with appropriate media over its entire length. Destabilization of the parallel orientation of BBC16 also occurs when hemes or Zn-protopophyrin IX are bound to BBC16. This makes the plateau of the BBC16 isotherm less flat, and we observe an intermediate orientation, in which both helices lie parallel to the interface but with one helix at the interface and the other helix beneath it in the subphase.[8] This is because ligation of the metalloporphyrin constrains the orientation of the helices of BBC16, keeping the nonpolar faces apposed, which would interfere with the dihelices' ability to keep their polar and nonpolar surfaces in contact with appropriate media. Binding heme to AP0 diminishes the plateau and removes the second inflection point from the isotherm.

As stated before, AP0 at high surface pressure is stable enough to sustain X-ray reflectivity experiments at constant area, rather than at constant pressure maintained by feedback control, as is necessary for BBC16. Figure 5b shows that the isotherm collected piece-wise (dotted) upon compression between reflectivity scans agrees well with the isotherms collected by continuous compression (solid). The hysteresis in the expansion isotherm is much smaller than that for BBC19.[9]

Structural Characterization by X-ray Reflectivity. With reference to the isotherms described above, normalized X-ray reflectivity data $R(q_z)/R_F(q_z)$ for the pure apo-AP0 peptide monolayer at four different pressures are shown in Figure 6a. At the lowest π of 10 mN/m, the data consist of a single broad maximum for momentum transfer $q_z < 0.7$ Å^{-1}. With increasing surface pressure, the maximum narrows and shifts to smaller q_z, developing subsidiary maxima/minima at the highest pressure investigated, 45 mN/m. In Figure 6b, the inverse Fourier transforms of these data are shown, which correspond to the autocorrelation of the gradient electron density profiles of the Langmuir monolayer at the four surface pressures. From these autocorrelation functions, it can be readily seen that the thickness, or maximum extent, of the gradient profile of the monolayer increases dramatically between 30 and 45 mN/m. Specifically, below 30 mN/m, the gradient electron density profile (and similarly, its integral, the electron density profile itself) contains no features separated by more than 20−30 Å, while at 45 mN/m the gradient profile contains features separated by as much as 50−60 Å, since the respective autocorrelation functions possess significant features of nonzero amplitude only for z-values less than separations indicated. Figure 6c shows the electron density profiles themselves derived from the normalized reflectivity data via the box-refinement method, requiring no *a priori* assumptions. At the lowest surface pressure of 10 mN/m, the single maximum in the electron density profile at the air−water interface is consistent with the cross-sectional profile of a single α-helix, indicating that the dihelices are oriented with the long axis of both helices lying in the plane of the air−water interface, that is, the plane of the dihelix lies in the plane of the interface. At a pressure of 30 mN/m, this single maximum broadens into the subphase by a factor of 2 times, indicating the dihelices have rotated 90° about their long axis such that while the long axis of each helix remains parallel to the plane of the interface, the plane of the dihelix is perpendicular to the plane of the interface. Finally, at π of 45 mN/m, the electron density profile of the monolayer of AP0 contains a broad plateau extending about 60 Å into the subphase, being relatively uniform over 50 Å of this length. This is consistent with the long axis of the helices being oriented perpendicular to the interface. For this particular amphiphilic peptide AP0, both the autocorrelation function of the gradient electron density profile and the electron density profile itself indicate that the entire ensemble has achieved this orientation at the highest surface pressure (since there remains no residual evidence of helices lying in the plane of the interface within either the autocorrelation function or the profile). The nature of this surface-pressure-dependent orientational transition is shown schematically in Figure 6d. Each helix of AP0 has 42 residues, excluding the 3 residues at the C-terminus forming the loop linking the two helices of the dihelix, which provides a length of 63 Å for a perfect straight α-helix at 1.5 Å/residue along the long axis. The small difference between the observed thickness of the monolayer (∼60 Å) and the calculated length could be attributed to a small tilt of the helices relative to the normal to the plane of the interface consistent with the somewhat larger than minimal area/helix at the highest surface pressure investigated. How-

(35) Gibney, B. R.; Isogai, Y.; Rabanal, F.; Reddy, K. S.; Grosset, A. M.; Moser, C. C.; Dutton, P. L. *Biochemistry* **2000**, *39*, 11041−11049.
(36) Gibney, B. R.; Rabanal, F.; Reddy, K. S.; Dutton, P. L. *Biochemistry* **1998**, *37*, 4635−4643.
(37) Skalicky, J. J.; Gibney, B. R.; Rabanal, F.; Urbauer, R. J. B.; Dutton, P. L.; Wand, A. J. *J. Am. Chem. Soc.* **1999**, *121*, 4941−4951.

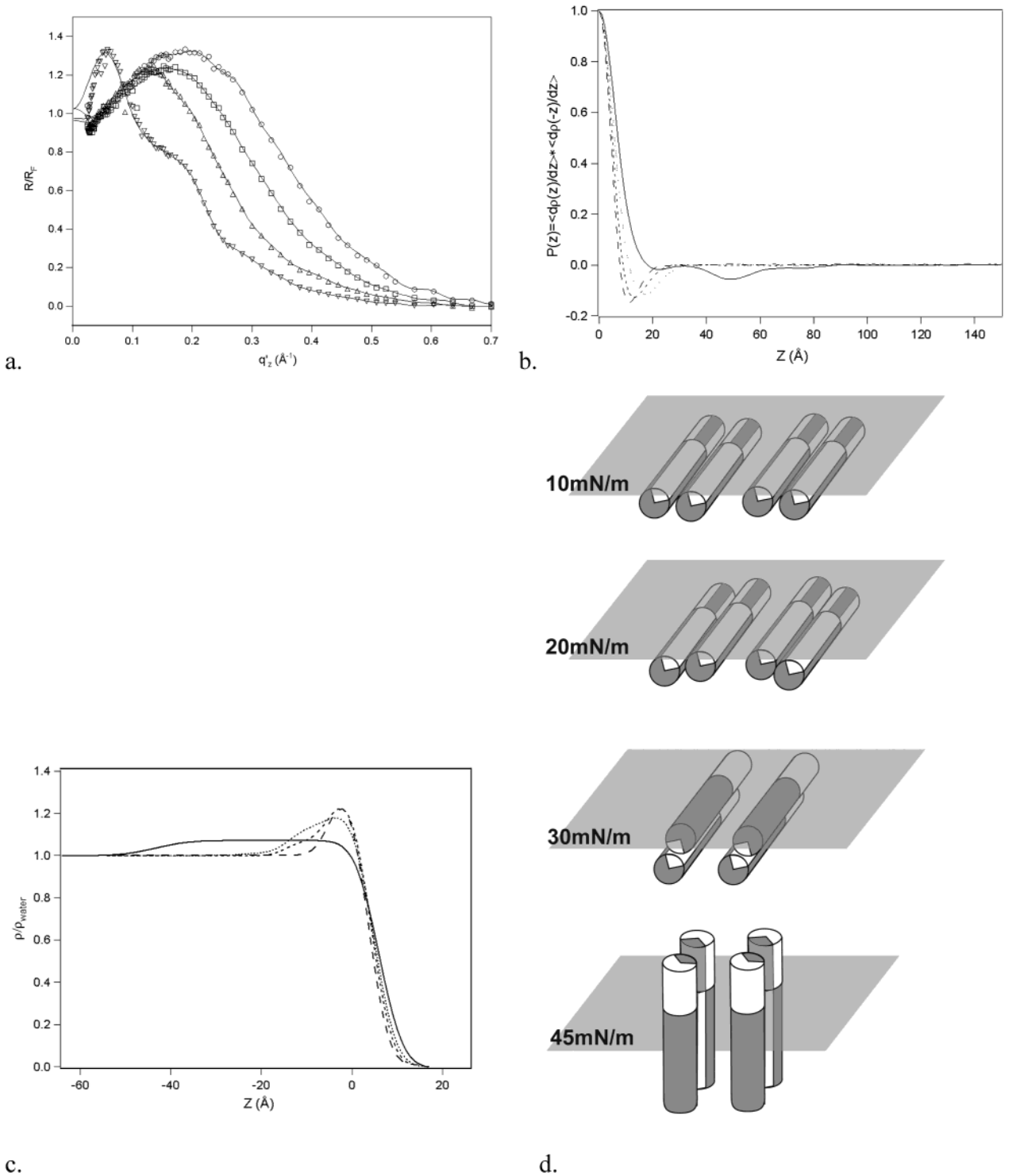

Figure 6. (a) Fresnel normalized X-ray reflectivity data collected from an AP0 monolayer at surface pressures (π) of 10 (○), 20 (□), 30 (△), and 45 mN/m (▽). The curves are calculated from the box-refinement result for the gradient profiles (not shown). (b) The Patterson or autocorrelation function of the monolayer gradient electron density profile computed from the data in part a at π =10 (long dash), 20 (short dash), 30 (dot), and 45 mN/m (solid). (c) The absolute electron density profiles for the monolayer at each pressure (same symbols as in part b) computed by analytic integration of a sum of Gaussian functions that best fit the gradient profiles from box refinement. (d) Schematic illustration of the surface-pressure-dependent orientational transition of apo-AP0 at the air−water interface; the air−water interface is indicated by the plane. At lower surface pressures of 10, 20, and 30 mN/m, both the autocorrelation functions and electron density profiles indicate that the long axis of the helices lies parallel to the interface, although the plane of the dihelices rotates from parallel to perpendicular to the interface with increasing pressure. When the pressure reaches 45 mN/m, both the autocorrelation function and the electron density profile indicate that all of the AP0 helices orient with their long axis normal to the plane of the air/water interface. However, although the packing of the dihelices in the plane of the interface at each of the various pressures investigated is relatively dense, irrespective of the different pressure-dependent orientations of the dihelices as indicated, the electron density profiles themselves for the monolayers cannot address the nature of the association of the dihelices in the plane of the interface.

ever, if the helices were indeed oriented with their long axis perfectly normal to the plane of the interface, then the uniformity of the monolayer electron density profile over 45−50 Å would suggest that only 30−33 residues

were α-helical (i.e., 71−79%) with those nearer the amino-terminus deepest in the aqueous subphase being somehow disordered perhaps by some unwinding of the helices. This is consistent with the circular dichroism data. We note that entirely similar results were obtained when the disulfide linkage forming the dihelices was not present. This indicates that the amphipathic helices associate to form dihelices even in the absence of the disulfide linkage. Also, entirely similar results were obtained for the holo-AP0 with one heme/4-helix bundle. These results are also similar to those obtained previously for BBC16, taking into account the different lengths of the helices for BBC16 (28 residues) versus AP0 (42 residues).

These profiles themselves can provide no direct evidence for the formation of 4-helix bundles at the interface. This can only be provided via X-ray scattering with momentum transfer parallel to the plane of the interface (a considerably more difficult experiment due to the small in-plane electron density contrast within the peptide monolayer).

Conclusions

The assembly and chemical and physical characterization of one prototypical member of a family of amphiphilic 4-helix bundle maquette peptides designed to generate vectorial function across an interface between polar and nonpolar media have been described. Other members of this family of maquette peptides as well as their vectorial incorporation into soft interfaces between polar and nonpolar media as provided by lipid monolayers and bilayers are described in separate communications. This provides the essential basis for future studies of the manifestation of their designed microscopic electrochemical and electro-optical properties in the macroscopic behavior of the interface as biomolecular materials.

Acknowledgment. The authors thank Andrey Tronin for assistance with data collection; Mike Sullivan for use of the support lab at beamline X9; Benjamin M. Ocko, Elaine DiMasi, and Scott Coburn for technical assistance at beamline X22-B at the National Synchrotron Light Source, Brookhaven National Laboratory (NSLS/BNL); and Ivan Kuzmenko and Thomas Gog for technical assistance at Sector 9 at the Advanced Photon Source, Argonne National Laboratory (APS/ANL). This work was supported by the National Institutes of Health under Grants GM48130, GM41048, GM63388, and GM55876 and by the MRSEC Program of the National Science Foundation under Award Number DMR96-32598. The NSLS/BNL and APS/ANL are supported by the U.S. Department of Energy.

LA0363884